

Inter-edge spin resonance in the Kitaev quantum spin liquid

Takahiro Misawa,¹ Joji Nasu,² and Yukitoshi Motome³

¹*Beijing Academy of Quantum Information Sciences, Haidian District, Beijing 100193, China*

²*Department of Physics, Tohoku University, Sendai 980-8578, Japan*

³*Department of Applied Physics, University of Tokyo, Tokyo 113-8656, Japan*
(Dated: April 4, 2023)

The Kitaev model offers a platform for quantum spin liquids (QSLs) with fractional excitations, itinerant Majorana fermions and localized fluxes. Since these fractional excitations could be utilized for quantum computing, how to create, observe, and control them through the spin degree of freedom is a central issue. Here, we study dynamical spin transport in the Kitaev-Heisenberg model by applying an AC magnetic field to an edge of the system. We find that, in the Kitaev QSL phase, spin polarizations at the other edge are resonantly induced in a specific spin component, even though the static spin correlations are vanishingly small. This inter-edge spin resonance appears around the input frequency over the broad frequency range. Comparing with the dynamical spin correlations, we clarify that the resonance is governed by the itinerant Majorana fermions with a broad continuum excitation spectrum, which can propagate over long distances, although it vanishes for the pure Kitaev model because of accidental degeneracy and requires weak Heisenberg interactions. We also find that the spin polarizations in the other spin components are weakly induced at an almost constant frequency close to the excitation gap of the localized fluxes, irrespective of the input frequency. These results demonstrate that the dynamical spin transport is a powerful probe of the fractional excitations in the Kitaev QSL. Possible experimental realization of the inter-edge spin resonance is discussed.

I. INTRODUCTION

Exotic quasiparticles emerging in solids have attracted much interest from both fundamental physics and industry applications. A prominent example is Majorana particles — charge-neutral spin-1/2 particles that are their own antiparticles^{1,2}. While they usually behave as fermions, in some two-dimensional cases they can be regarded as anyons that obey neither Fermi-Dirac nor Bose-Einstein statistics. Such Majorana particles have been intensively studied for applications to quantum computing by using the anyonic nature^{3,4}.

The Kitaev model on a honeycomb lattice offers an ideal platform for realizing the Majorana particles⁵. It is an exactly solvable model whose ground state is a quantum spin liquid (QSL). The Kitaev QSL hosts two types of emergent quasiparticles from the fractionalization of spins: itinerant Majorana fermions and localized fluxes. These quasiparticles turn into Abelian anyons when the interactions between spins are largely anisotropic, or non-Abelian anyons when an external magnetic field is applied in the nearly isotropic cases^{3,5}. The Kitaev model could be realized in Mott insulators with the strong spin-orbit coupling⁶, such as Na_2IrO_3 ⁷ and $\alpha\text{-RuCl}_3$ ⁸. Detailed comparisons between experimental results and theoretical calculations have revealed fingerprints of the Majorana particles in such candidate materials; for a review, see Ref. 9. Among them, the discovery of the half-quantized thermal Hall effect in $\alpha\text{-RuCl}_3$ was ground breaking, providing direct evidence for the Majorana particles^{10–12}, while it is still under debate^{13–15}.

Since the Majorana fermions and the fluxes in the Kitaev QSL are generated by the fractionalization of spins, they are quantum entangled and inherently nonlocal.

Indeed, the spatial correlations between the Majorana fermions are long-range with power-law decay^{16,17}, although the spin correlations are short-ranged and vanish beyond nearest-neighbor sites¹⁸. It was also shown that the itinerant Majorana fermions induce long-range spin transport¹⁹. Furthermore, in the presence of defects or edges, the spin correlations can be long-range due to low-energy excitations around the defects or edges and the nonlocal nature of the fractional quasiparticles^{16,17,20–22}. Toward quantum computing, it is crucially important to elucidate how to control and probe such nonlocality via the spin degree of freedom, but it is not fully clarified yet in spite of many theoretical works^{23–32}.

In this paper, in order to understand the relationship between the fractional quasiparticles and the spin degree of freedom, we study nonlocal spin dynamics in the Kitaev QSL. In particular, we consider the systems with edges and examine how the spin excitations propagate from one edge to the other. At the edges of the Kitaev model, it is known that local magnetic fields excite the fluxes accompanied by gapless Majorana excitations, called the Majorana zero modes^{5,16}. In the present study, we introduce not static but time-dependent local magnetic fields at one edge and investigate how the excited spin polarizations propagate through the system. From the analysis, we clarify the relationship between the fractional excitations and the nonlocal dynamical correlations in the spin degree of freedom, which gives an insight on the way of creation and control of the fractional excitations via the spin degree of freedom.

The organization of this paper is as follows. In Sec. II, we introduce the model and the setup used in this study, with the details of real-time evolution and the definitions of static and dynamical spin correlations. In Sec. III A,

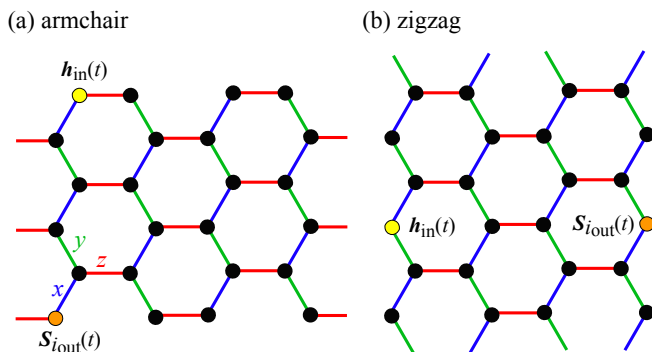


FIG. 1. Schematic pictures of the Kitaev-Heisenberg model in Eq. (1) with (a) the armchair edges and (b) the zigzag edges. In (a) [(b)], we set the periodic and open (open and periodic) boundary conditions in the horizontal and vertical directions, respectively. The blue, green, and red bonds represent the x , y , and z bonds for the Kitaev interaction, respectively. We apply an AC magnetic field $\mathbf{h}_{\text{in}}(t)$ in the $[111]$ direction in spin space at one site on the edge shown by the yellow circles, and observe spin polarization at a site on the opposite edge shown by the orange circles; see Eqs. (3), (4), and (6).

we show the phase diagram and the static spin correlations in our model with edges. In Sec. III B, we show how an AC local magnetic field at the edge induces the spin polarization at the opposite edge of the system in the ferromagnetic phase, the Kitaev QSL, and the stripy phase. In Sec. III C, we analyze the results in comparison with the dynamical spin correlations between edges, and discuss the origin of the inter-edge dynamical spin transport. Section IV is devoted to a summary.

II. MODEL AND METHOD

In this paper, we employ the Kitaev-Heisenberg model, whose Hamiltonian is given by

$$\hat{\mathcal{H}}_{\text{KH}} = K \sum_{\nu} \sum_{\langle i,j \rangle_{\nu}} \hat{S}_i^{\nu} \hat{S}_j^{\nu} + J \sum_{\langle i,j \rangle} \hat{\mathbf{S}}_i \cdot \hat{\mathbf{S}}_j, \quad (1)$$

where \hat{S}_i^{ν} denotes the ν th component of the spin-1/2 operator at i th site: $\hat{\mathbf{S}}_i = (\hat{S}_i^x, \hat{S}_i^y, \hat{S}_i^z)$. The first term represents the bond-dependent Ising-type interaction, called the Kitaev interaction, where $\langle i,j \rangle_{\nu}$ represents the nearest-neighbor $\nu (= x, y, z)$ bonds on the honeycomb lattice, and the second term represents the spin-isotropic Heisenberg interaction for all the nearest-neighbor bonds; see Fig. 1. Following the previous studies^{7,33}, we parametrize the two coupling constants as

$$(K, J) = \left(\sin \alpha, \frac{1}{2} \cos \alpha \right). \quad (2)$$

Note that the amplitudes of interactions are halved compared to the previous ones so that $|K| = 1$ in the pure

Kitaev cases with $\alpha = \pi/2$ and $3\pi/2$. In the following, we focus on the range of $\pi \leq \alpha \leq 7\pi/4$ where the Kitaev interaction is ferromagnetic. In this region, the bulk system with the periodic boundary conditions shows three phases in the ground state³³: the ferromagnetic phase for $\pi \leq \alpha \lesssim 1.40\pi$, the Kitaev QSL phase for $1.40\pi \lesssim \alpha \lesssim 1.58\pi$, and the stripy phase for $1.58\pi \lesssim \alpha \lesssim 1.81\pi$.

To study spin correlations and dynamics on the edges, we consider the model in Eq. (1) on a strip with the open boundary condition in one direction and the periodic boundary condition in the other. There are two types of such strips. One has the so-called armchair type edges on the open boundaries, and the other has the so-called zigzag edges. Figure 1 displays these two types for 24-site clusters used in the following calculations. For both clusters, we examine how a time-dependent local magnetic field on one edge induces spin polarization at the other edge. Specifically, we apply an AC magnetic field in the $[111]$ direction in spin space at i_{in} th site on the edge (shown by the yellow circle in Fig. 1) as

$$\hat{\mathcal{H}}(t) = \hat{\mathcal{H}}_{\text{KH}} + \mathbf{h}_{\text{in}}(t) \cdot \hat{\mathbf{S}}_{i_{\text{in}}}, \quad (3)$$

with

$$\mathbf{h}_{\text{in}}(t) = h \mathbf{e}_c \cos(\Omega t), \quad (4)$$

where h is the amplitude of the AC field, $\mathbf{e}_c = (1, 1, 1)/\sqrt{3}$, and $\Omega = 2\pi/T$ is the frequency of the AC field (T represents the oscillation period). For this Hamiltonian, we solve the time-dependent Schrödinger equation given by

$$i \frac{d|\Phi(t)\rangle}{dt} = \hat{\mathcal{H}}(t) |\Phi(t)\rangle, \quad (5)$$

starting from the initial condition of $|\Phi(t=0)\rangle = |\Phi_{\text{GS}}\rangle$, where $|\Phi_{\text{GS}}\rangle$ is the normalized ground state of $\hat{\mathcal{H}}_{\text{KH}}$. The spin polarization on the opposite edge is calculated as

$$S_{i_{\text{out}}}^{\nu}(t) = \langle \Phi(t) | \hat{S}_{i_{\text{out}}}^{\nu} | \Phi(t) \rangle, \quad (6)$$

where i_{out} denotes the site on the other edge directly opposite to the i_{in} th site (shown by the orange circle in Fig. 1). In the following calculations, we take $h = 0.05$ in Eq. (4) and solve Eq. (5) by using $\mathcal{H}\Phi$ ³⁴; we discretize the time with $\Delta t = 0.05$, which is small enough to preserve the unitarity of real-time evolution.

In addition to the real-time dynamics of the spin polarization, we calculate the static and dynamical spin correlations between the two edges for the ground state $|\Phi_{\text{GS}}\rangle$, which are defined by

$$S_{\text{edge}}^{\nu\nu} = \langle \Phi_{\text{GS}} | \hat{S}_{i_{\text{in}}}^{\nu} \hat{S}_{i_{\text{out}}}^{\nu} | \Phi_{\text{GS}} \rangle, \quad (7)$$

and

$$S_{\text{edge}}^{\nu\nu}(\omega) = \frac{1}{2\pi} \int_{-\infty}^{\infty} \langle \Phi_{\text{GS}} | \delta \hat{S}_{i_{\text{in}}}^{\nu}(t) \delta \hat{S}_{i_{\text{out}}}^{\nu} | \Phi_{\text{GS}} \rangle e^{i\omega t} dt, \quad (8)$$

respectively, where $\delta\hat{S}_i^\nu = \hat{S}_i^\nu - \langle\Phi_{\text{GS}}|\hat{S}_i^\nu|\Phi_{\text{GS}}\rangle$ and $\delta\hat{S}_{i_{\text{in}}}^\nu(t) = e^{i\hat{H}_{\text{KH}}t}\delta\hat{S}_{i_{\text{in}}}^\nu e^{-i\hat{H}_{\text{KH}}t}$. Note that in Eq. (8) we consider correlations between the deviations from the expectation values for the ground state to subtract the elastic components in the presence of magnetic ordering. In the actual calculations of Eq. (8), we employ the following formula in the spectral representation:

$$S_{\text{edge}}^{\nu\nu}(\omega) = -\frac{1}{4\pi}\text{Im}\left[\langle\Psi_+|(E_{\text{GS}} - \hat{H}_{\text{KH}} + \omega + i\eta)^{-1}|\Psi_+\rangle - \langle\Psi_-|(E_{\text{GS}} - \hat{H}_{\text{KH}} + \omega + i\eta)^{-1}|\Psi_-\rangle\right], \quad (9)$$

where $|\Psi_\pm\rangle = (\delta\hat{S}_{i_{\text{in}}}^\nu \pm \delta\hat{S}_{i_{\text{out}}}^\nu)|\Phi_{\text{GS}}\rangle$, E_{GS} is the ground-state energy, and η is an infinitesimal positive constant; we take $\eta = 0.05$ in the following calculations. We calculate Eq. (9) using the continued-fraction expansion based on the Lanczos method.

In the calculations of Eqs. (7) and (9), we apply a weak static magnetic field to all the spins at the edge on the i_{in} th side with $\mathbf{h}_s = 0.005\mathbf{e}_c$ to lift the ground-state degeneracy in the ferromagnetic Heisenberg model with $\alpha = \pi$ and the pure Kitaev model with $\alpha = 3\pi/2$ (see Appendix A). For the other cases, the ground state is not degenerate, but we apply the same weak field for comparison.

III. RESULTS

A. Phase diagram and static spin correlations

Before going into the spin dynamics, we discuss the ground states of the clusters with edges shown in Fig. 1. Figures 2(a) and 2(b) show the α dependences of the second derivative of the ground-state energy for the systems with the armchair and zigzag edges, respectively. The two peaks at $\alpha = \alpha_{c1}$ and $\alpha = \alpha_{c2}$ indicate first-order phase transitions. Figures 2(c) and 2(d) display the static inter-edge spin correlations defined by Eq. (7). From these data, we identify three different phases: the ferromagnetic phase with a positive spin correlation for $\alpha < \alpha_{c1}$, the Kitaev QSL with almost zero correlation for $\alpha_{c1} < \alpha < \alpha_{c2}$, and the stripy phase with a negative (positive) correlation for the system with the armchair (zigzag) edges for $\alpha > \alpha_{c2}$. The antiferromagnetic and ferromagnetic spin correlations in the stripy phase are understood from the schematic pictures in Figs. 2(e) and 2(f), respectively. We note that in the ferromagnetic and stripy phases the spin correlations are dominant in a specific spin component S^z due to the presence of edges, except for $\alpha = \pi$ where the ground state is degenerate in the absence of the weak magnetic field \mathbf{h}_s .

Our phase diagrams obtained for the clusters with edges are nearly identical to that for the same size cluster under the periodic boundary conditions³³. For the

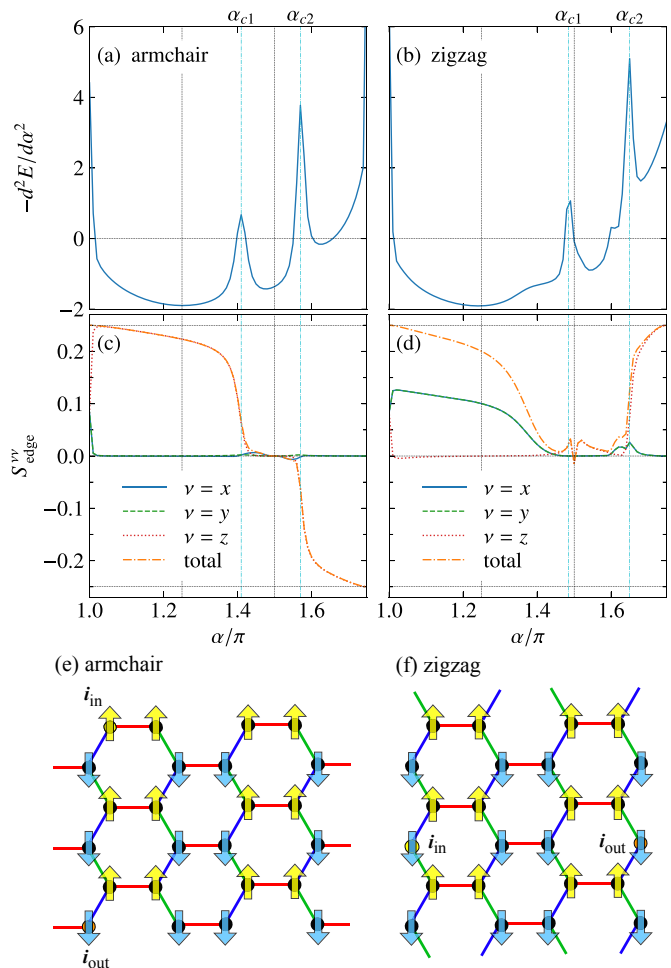


FIG. 2. α dependences of the second derivative of the ground-state energy for the systems with (a) the armchair edges and (b) the zigzag edges. Corresponding static inter-edge spin correlations are plotted in (c) and (d). (e) and (f) show the schematic pictures of the stripy order in the case of armchair and zigzag edges, respectively.

system with the armchair (zigzag) edges, we find that the phase boundary between the ferromagnetic and Kitaev QSL phases is at $\alpha_{c1} \simeq 1.41\pi$ (1.49π) and that between the Kitaev QSL and stripy phases is at $\alpha_{c2} \simeq 1.57\pi$ (1.65π). These estimates are close to those for the clusters with the periodic boundary conditions, $\alpha_{c1} \simeq 1.40\pi$ and $\alpha_{c2} \simeq 1.58\pi$ ³³. This indicates that the bulk properties are not much affected by the introduction of edges even for clusters of this size. In the following sections, we will compute the spin dynamics in the three phases: For the ferromagnetic, Kitaev QSL, and stripy phases, we take $\alpha = 1.25\pi$, 1.52π , and 1.67π , respectively, for both cases of the armchair and zigzag edges.

Let us comment on the symmetry of the two clusters in Fig. 1. In the bulk system of the Kitaev-Heisenberg model, there is a four-sublattice transformation which

does not change the form of the Hamiltonian with replacing K and J by $K + J$ and $-J$, respectively³³. This transformation leads to the relation between the phase boundaries as $\tan \alpha_{c2} = -\tan \alpha_{c1} - 1$. In the system with the armchair edges, the relation holds for our estimates of α_{c1} and α_{c2} , since the cluster respects the four-sublattice symmetry. In contrast, in the case of the zigzag edges, the symmetry is lost, and α_{c1} and α_{c2} do not satisfy the relation.

B. Real-time spin dynamics

We now turn to discuss how the spin at the edge is polarized when the AC magnetic field is applied to the spin at the other edge. Below, we present the results for the systems with armchair and zigzag edges in Secs. III B 1 and III B 2, respectively, and discuss the inter-edge spin resonance in the Kitaev QSL in Sec. III B 3.

1. Armchair edge

Figure 3 displays the time evolution of spin polarization at the i_{out} th site in Eq. (6) for the system with armchair edges in Fig. 1(a). In the main panels, we show the results for the period of the oscillating field, $T = 10, 20, 40, 60,$ and 80 . Meanwhile, in the insets, we plot the Fourier transformed spectra obtained by

$$S^\nu(\omega) = \left| \frac{2}{t_{\text{max}}} \int_0^{t_{\text{max}}} S_{i_{\text{out}}}^\nu(t) e^{i\omega t} dt \right|, \quad (10)$$

where we take $t_{\text{max}} = 500$.

We first discuss the results in the ferromagnetic phase shown in Figs. 3(a)–3(c). In this case, both $S_{i_{\text{out}}}^x(t)$ and $S_{i_{\text{out}}}^y(t)$ show considerable oscillations, while $S_{i_{\text{out}}}^z(t)$ does not. These behaviors are understood from the spin ordering in the ground state: As shown in Fig. 2(c), the spins are ferromagnetically ordered in the z direction, for which fluctuations appear dominantly in the transverse components, $S_{i_{\text{out}}}^x$ and $S_{i_{\text{out}}}^y$, rather than the longitudinal one $S_{i_{\text{out}}}^z$. In the Fourier transformed spectra shown in the insets, we find that the dominant $S^x(\omega)$ and $S^y(\omega)$ always show a peak around $\omega = \Omega = 2\pi/T$. This result indicates that the spin polarization is induced dominantly at the same frequency of the input AC magnetic field.

Next, we turn to the results in the Kitaev QSL phase shown in Figs. 3(d)–3(f). In contrast to the above ferromagnetic case, we find that only $S_{i_{\text{out}}}^y(t)$ shows considerable oscillations, while the others do not. This behavior can be understood from the fractional excitations in the Kitaev QSL as follows. In the exact solution for the pure Kitaev model, as mentioned in Sec. I, the spins are fractionalized into itinerant Majorana fermions and localized fluxes. The former has gapless excitations, while the latter is gapped⁵. The spin excitation is a composite of these two, and hence gapped. Indeed, the spin excitations by

\hat{S}^x or \hat{S}^z at the i_{in} or i_{out} th site are gapped since these spin operators do not commute with the flux operators defined by products of six spins on the hexagons including the i_{in} or i_{out} th site⁵. This suppresses $S_{i_{\text{out}}}^x(t)$ and $S_{i_{\text{out}}}^z(t)$ in Figs. 3(d) and 3(f), respectively. In contrast, \hat{S}^y at the i_{in} or i_{out} th site commutes with the flux operators, since the hexagons lack the y bond. In addition to the hexagonal fluxes, in the cluster with the armchair edges, there are additional flux operators defined only by the edge spins. While \hat{S}^y at the i_{in} or i_{out} th site do not commute with these fluxes, the spin excitations remain gapless because of the degeneracy in the ground state (see Appendix A). These allow the excitation by $\hat{S}_{i_{\text{in}}}^y$ to yield long-range spin propagation via the gapless itinerant quasiparticles and induce $S_{i_{\text{out}}}^y(t)$ in Fig. 3(e). Although the above argument is valid only for the pure Kitaev case, similar behavior is expected to appear in the Kitaev QSL phase in the presence of weak Heisenberg interactions. This is the reason why only $S_{i_{\text{out}}}^y(t)$ shows significantly large oscillations in Figs. 3(d)–3(f).

The resonant behaviors in the Kitaev QSL phase exhibit the following characteristics. First, while $S^y(\omega)$ always shows a peak around the input frequency Ω as in the ferromagnetic case, the peak height does not decrease but rather increases with ω , as shown in the inset of Fig. 3(e). This characteristic behavior will be discussed in Sec. III B 3. Second, we note that a weak Heisenberg interaction is crucial for the long-range spin propagation since the ground state degeneracy in the pure Kitaev case with $\alpha/\pi = 1.5$ prohibits the propagation, as we will discuss in detail in Sec. III C. Finally, the above argument also allows static inter-edge spin correlation in the y direction, S_{edge}^{yy} , also to develop, but it is almost zero as shown in Fig. 2(c). This indicates that the inter-edge spin correlations in the Kitaev QSL can only be dynamically enhanced.

Lastly, we discuss the results in the stripy phase shown in Figs. 3(g)–3(i). In this case, the results are similar to the ferromagnetic case in Figs. 3(a)–3(c). The reason is common: As shown in Fig. 2(c), the spins are antiferromagnetically ordered in the z direction in this stripy phase, and hence, the transverse components $S_{i_{\text{out}}}^x(t)$ and $S_{i_{\text{out}}}^y(t)$ are induced dominantly at the input frequency.

2. Zigzag edge

Figure 4 displays the results for the system with the zigzag edges in Fig. 1(b), obtained by the same conditions for the armchair case. For the ferromagnetic and stripy phases shown in Figs. 4(a)–4(c) and 4(g)–4(i), respectively, we find similar tendency to the armchair case: The spin polarizations in the x and y directions are induced significantly, while that in the z direction is rather suppressed. This is again understood from the fact that the ordered moments in each phase appear in the z direction as shown in Fig. 2(d).

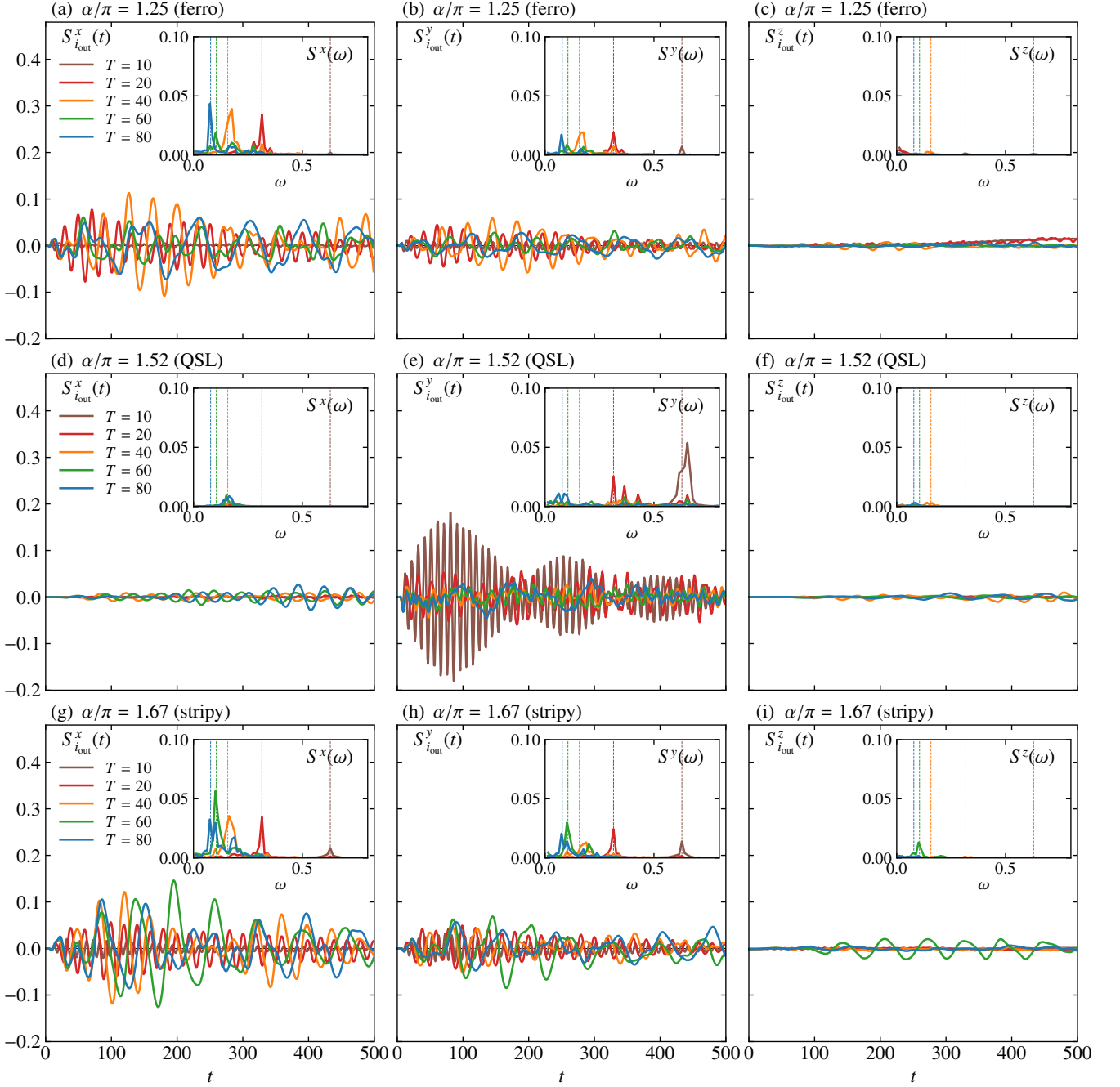


FIG. 3. Time evolution of the spin polarization $S_{i_{out}}^{\nu}(t)$ in Eq. (6) for the system with armchair edges in (a)–(c) the ferromagnetic phase at $\alpha/\pi = 1.25$, (d)–(f) the Kitaev QSL phase at $\alpha/\pi = 1.52$, and (g)–(i) the stripy phase at $\alpha/\pi = 1.67$: (a),(d),(g) $\nu = x$, (b),(e),(h) $\nu = y$, and (c),(f),(i) $\nu = z$. The data for the input oscillation periods $T = 10, 20, 40, 60$, and 80 are shown. The insets display the corresponding Fourier transformed spin polarizations in Eq. (10). The vertical dashed lines denote the frequencies corresponding to the values of T , $\omega = 2\pi/T$.

Meanwhile, in the Kitaev QSL phase, as shown in Figs. 4(d)–4(f), we find that $S_{i_{out}}^z(t)$ shows significant large oscillations, while $S_{i_{out}}^x(t)$ and $S_{i_{out}}^y(t)$ do not. This can also be understood from the flux excitations discussed above for the armchair case. In the current case,

the zigzag edges lack the z bonds, and hence, the S^z components can be excited without the gapped excitations owing to the ground state degeneracy; see Appendix A. Interestingly, the amplitude of $S_{i_{out}}^z(t)$ varies nonmonotonically with T and takes the maximum value around

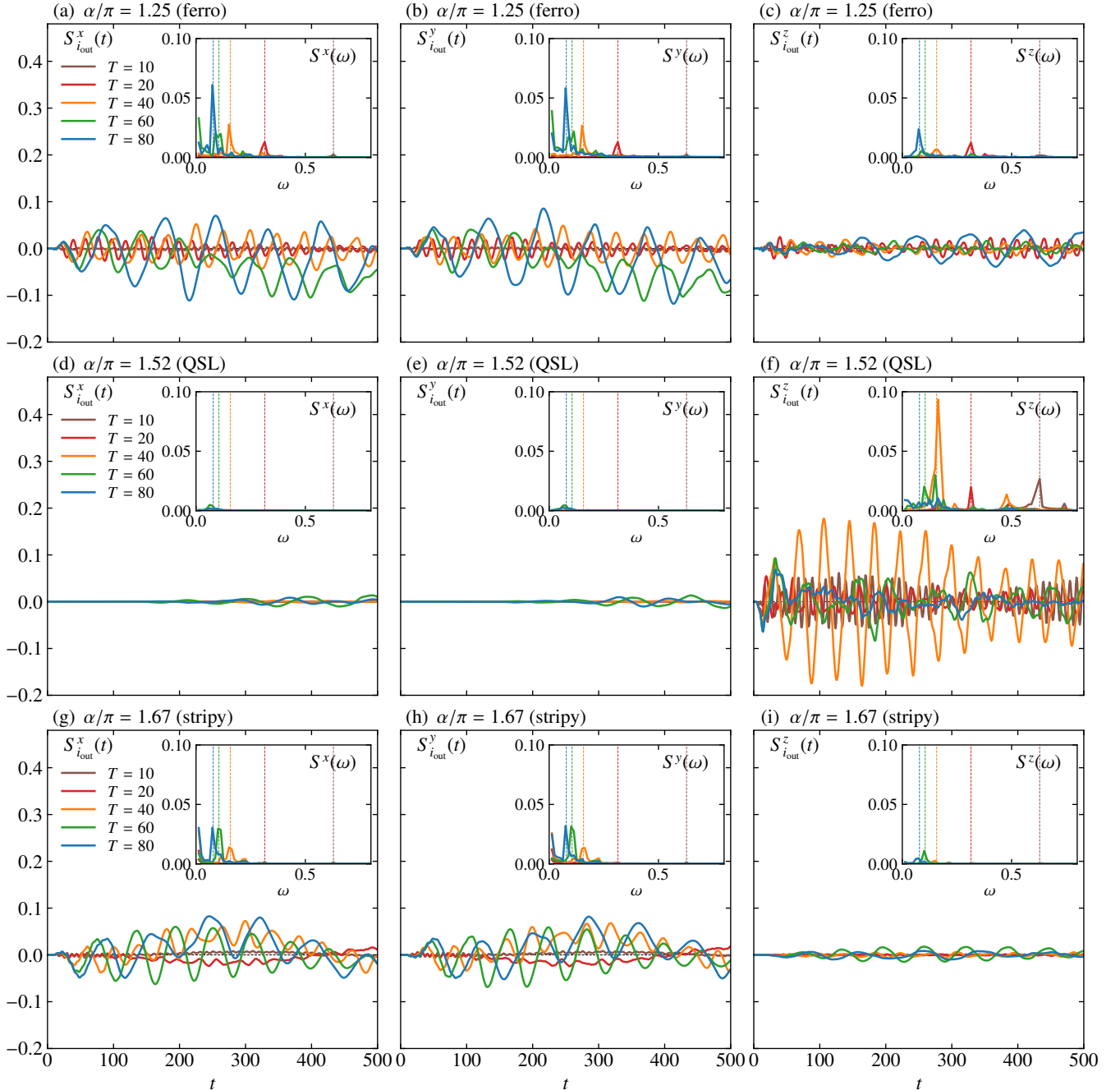


FIG. 4. Corresponding plots to Fig. 3 for the system with zigzag edges.

$T = 40$, as shown in Fig. 4(f). In this case also, we observe the peaks in $S^z(\omega)$ at almost the input frequencies, as shown in the inset of Fig. 4(f), while the peak heights show nonmonotonic ω dependence. These features will be discussed in the next section.

3. Inter-edge resonance

In Fig. 5, we show $\Omega = 2\pi/T$ dependences of the maximum values of $S^\nu(\omega)$ ($\nu = x, y, z$) within the range of $2/t_{\max} < \omega/2\pi \leq 0.5$, which are represented as $S^\nu(\omega_{\text{peak}})$, in the systems with (a)-(c) the armchair edges and (d)-(f) the zigzag edges. We also plot the values of ω_{peak} as functions of Ω in each inset.

In both armchair and zigzag cases, $S^x(\omega_{\text{peak}})$ and

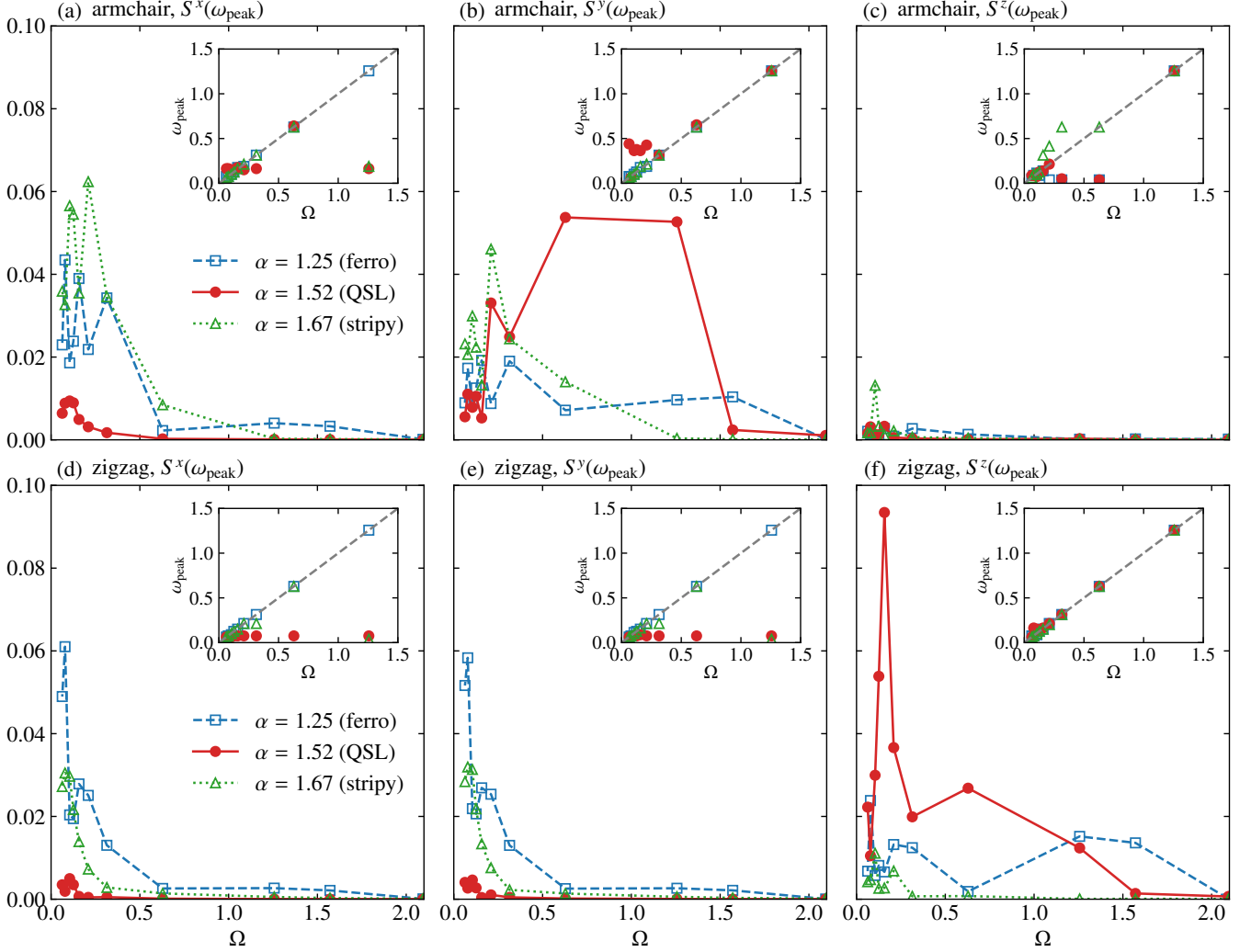


FIG. 5. Maximum values of the Fourier transformed spin polarizations $S^\nu(\omega_{\text{peak}})$ for the input oscillating magnetic field with $\Omega = 2\pi/T$ in the systems with (a)–(c) the armchair edges and (d)–(f) the zigzag edges: (a) and (d) $\nu = x$, (b) and (e) $\nu = y$, and (c) and (f) $\nu = z$. The insets display Ω dependences of ω_{peak} . The gray dashed line shows the relation $\omega_{\text{peak}} = \Omega$.

$S^y(\omega_{\text{peak}})$ have large values in the ferromagnetic and stripy phases, while $S^z(\omega_{\text{peak}})$ are suppressed, since these phases show the spin orderings along the z direction as mentioned above. The values of $S^x(\omega_{\text{peak}})$ and $S^y(\omega_{\text{peak}})$ decrease as Ω increases. In addition, we find that the values of ω_{peak} are close to Ω as shown in each inset. These are indications of conventional magnetic resonances; the spin polarization is induced dominantly at the input frequency, as long as the magnetic excitations are available in the frequency range.

In contrast, the inter-edge spin resonance behaves differently in the Kitaev QSL phase. First of all, we find that the dominant polarizations, $S^y(\omega_{\text{peak}})$ for the armchair case and $S^z(\omega_{\text{peak}})$ for the zigzag case, show broad peaks in the wide frequency range up to $\Omega \simeq 1.5$, while the latter shows a sharp peak at a smaller $\Omega \simeq 0.2$ as well. For both cases, the relation $\omega_{\text{peak}} \sim \Omega$ holds, except for

small Ω ($\Omega \lesssim 0.2$ for the armchair case and $\Omega \lesssim 0.1$ for the zigzag case); the deviation might be due to the finite-size effect. The broad responses with $\omega_{\text{peak}} \sim \Omega$, as well as the sharp peak in the zigzag case, can be ascribed to the itinerant Majorana fermions, whose density of states shows a continuum up to $\omega = 1.5^5$. This point will be further discussed in Sec. III C.

In addition, for the other spin components with suppressed polarizations, we find that ω_{peak} is almost constant irrespective of Ω^{35} . This behavior could be explained by the flux gap that governs the low-energy excitations in these spin components. We note that the constant values of $\omega_{\text{peak}} \sim 0.2$ in the armchair case is larger than the energy of the low-energy coherent peak at $\omega \sim 0.1$ in the dynamical spin structure factor of the pure Kitaev model in the thermodynamic limit³⁶, but this might also be due to the finite-size effect.

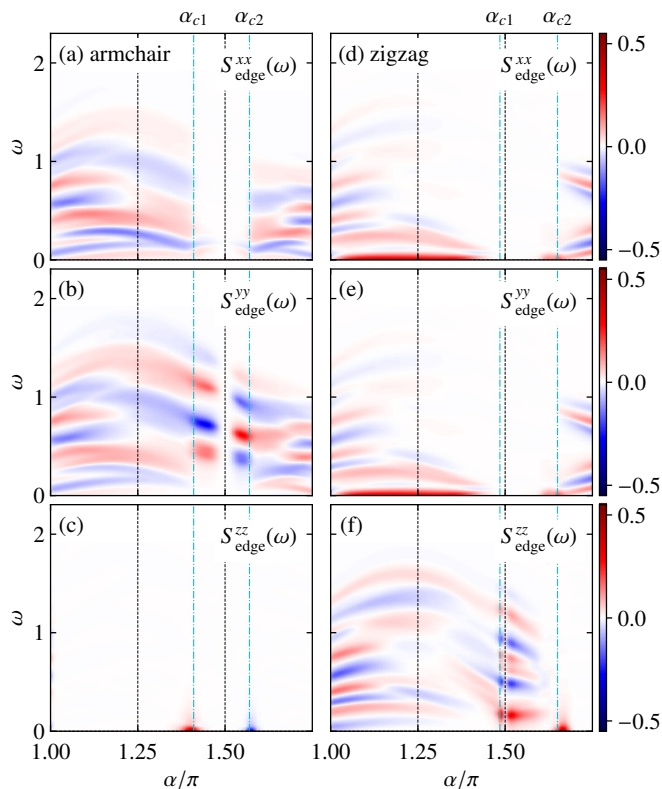


FIG. 6. Dynamical inter-edge spin correlations $S_{\text{edge}}^{\nu\nu}(\omega)$ [Eq. (8)] for (a),(c),(e) the armchair edge and (b),(d),(f) the zigzag edge: (a) and (b) $\nu = x$, (c) and (d) $\nu = y$, and (e) and (f) $\nu = z$.

In the Kitaev QSL, $S^x(\omega_{\text{peak}})$ is larger than $S^z(\omega_{\text{peak}})$ in the armchair case, while $S^x(\omega_{\text{peak}})$ and $S^y(\omega_{\text{peak}})$ are almost the same in the zigzag case. This is understood from the geometry of the Kitaev bonds in each cluster. In the armchair case, as shown in Fig. 1(a), the z bonds on which \hat{S}^z components interact via the Kitaev interaction are along the edges and perpendicular to the direction from i_{in} to i_{out} , which may suppress the inter-edge spin transport of the z component. Meanwhile, in the zigzag case shown in Fig. 1(b), both x and y bonds are along the edges and related with each other by symmetry, leading to almost the same inter-edge resonances assisted by the z bonds connecting them.

C. Comparison with dynamical spin correlations

Let us discuss the characteristic inter-edge spin resonances in comparison with the dynamical inter-edge spin correlations $S_{\text{edge}}^{\nu\nu}(\omega)$ defined in Eq. (8). Figure 6 displays $S_{\text{edge}}^{\nu\nu}(\omega)$ for the armchair and zigzag cases while varying α . In the following, we show that $S_{\text{edge}}^{\nu\nu}(\omega)$ explains well the intensities and Ω dependences of the induced spin polarizations in Fig. 5.

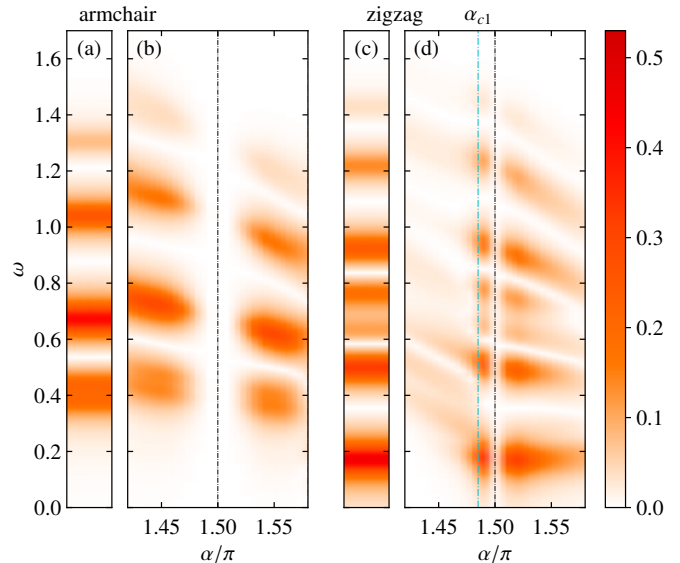


FIG. 7. Comparison between (a) $|S_{\text{edge}}^{\text{Maj}}(\omega)|$ calculated by Eq. (B3) for the pure Kitaev model at $\alpha/\pi = 1.5$ and (b) an enlarged plot of $|S_{\text{edge}}^{yy}(\omega)|$ around $\alpha/\pi = 1.5$ for the system with the armchair edges. (c) and (d) The corresponding plots for the zigzag case, where $|S_{\text{edge}}^{zz}(\omega)|$ is plotted in (d).

In the system with armchair edges, $S_{\text{edge}}^{xx}(\omega)$ and $S_{\text{edge}}^{yy}(\omega)$ show considerable intensities over the broad ω range, whereas $S_{\text{edge}}^{zz}(\omega)$ is almost zero except for the low- ω weights near the phase boundaries at $\alpha = \alpha_{c1}$ and α_{c2} . In the ferromagnetic phase for $\alpha \leq \alpha_{c1}$ and the stripy phase for $\alpha \geq \alpha_{c2}$, this is again consistent with the fact that the spin moments are ordered along the z direction. A striking difference between $S_{\text{edge}}^{xx}(\omega)$ and $S_{\text{edge}}^{yy}(\omega)$ appears in the Kitaev QSL phase for $\alpha_{c1} \leq \alpha \leq \alpha_{c2}$; $S_{\text{edge}}^{yy}(\omega)$ has large spectral weights over the broad ω range, while $S_{\text{edge}}^{xx}(\omega)$ is almost zero. Notably, the intensity of $S_{\text{edge}}^{yy}(\omega)$ is stronger than those in the ferromagnetic and stripy phases, while it vanishes for the pure Kitaev case at $\alpha/\pi = 1.5$ because of the degeneracy in the ground state (see Appendix B). This strong $S_{\text{edge}}^{yy}(\omega)$ explains well the broad response in $S^y(\omega_{\text{peak}})$ found in Fig. 5(b). In addition, we note that $S_{\text{edge}}^{xx}(\omega)$ has weak intensities at low $\omega \sim 0.1$, as shown in Fig. 6(a). This also explains well the small peak in $S^x(\omega_{\text{peak}})$ found in Fig. 5(a).

Meanwhile, in the system with zigzag edges, $S_{\text{edge}}^{\nu\nu}(\omega)$ in the ferromagnetic and stripy phases behave qualitatively similarly to those in the armchair case. In the Kitaev QSL phase, however, strong intensity appears in $S_{\text{edge}}^{zz}(\omega)$ over the broad ω range, while $S_{\text{edge}}^{xx}(\omega)$ and $S_{\text{edge}}^{yy}(\omega)$ are almost absent. Again, this explains well the broad response in $S^z(\omega_{\text{peak}})$ found in Fig. 5(f). Furthermore, the sharp peak at $\omega \sim 0.2$ in Fig. 5(f) is also consistent with the strong intensity of $S_{\text{edge}}^{zz}(\omega)$ in Fig. 6(f).

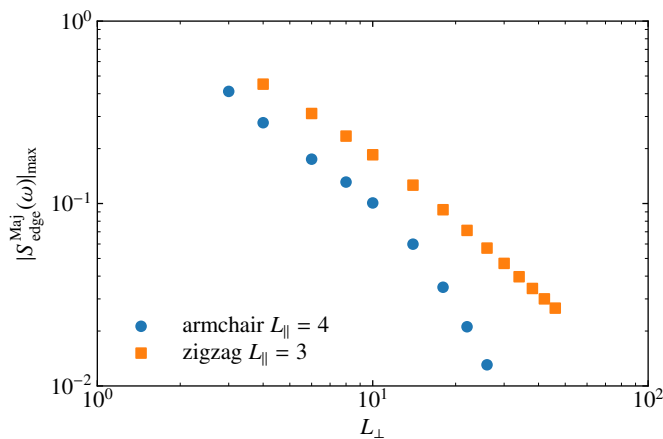


FIG. 8. Maximum of $|S_{edge}^{Maj}(\omega)|$ as a function of the number of the unit cells in the direction perpendicular to the edges, L_{\perp} . The data are calculated for the clusters with the numbers of the unit cell along the edge, $L_{\parallel} = 4$ and 3 , for the armchair and zigzag cases, respectively; the result for the smallest L_{\perp} in each case corresponds to that in Figs. 7(a) and 7(c).

The inter-edge resonances in the broad ω range in the Kitaev QSL phase are mediated by the itinerant Majorana fermions whose excitation spectrum has a continuum in the broad energy range. This is explicitly shown by calculating the dynamical spin correlations for the pure Kitaev model at $\alpha/\pi = 1.5$ by using the Majorana representation, which we denote $S_{edge}^{Maj}(\omega)$; see Appendix B for the details of the calculations. Figure 7 shows the results of $S_{edge}^{Maj}(\omega)$ in comparison with $S_{edge}^{yy}(\omega)$ and $S_{edge}^{zz}(\omega)$ around $\alpha/\pi = 1.5$. Note that here we compare their absolute values since the sign of $S_{edge}^{Maj}(\omega)$ in Eq. (B3) is not well defined. We find that the broad responses of $S_{edge}^{yy}(\omega)$ and $S_{edge}^{zz}(\omega)$ in the vicinity of $\alpha/\pi = 1.5$ appear in the same energy range of $S_{edge}^{Maj}(\omega)$ with showing similar ω dependences. This indicates that the broad responses in the Kitaev QSL phase are dominated by the itinerant Majorana excitations.

While our results are limited to the small clusters, we expect that the inter-edge resonances appear also in larger systems since the itinerant Majorana fermions propagate over long distances in the Kitaev QSL. This is demonstrated by calculating $|S_{edge}^{Maj}(\omega)|$ while changing the system width. Figure 8 shows the maximum intensity of $|S_{edge}^{Maj}(\omega)|$ as a function of the number of the unit cells in the direction perpendicular to the edges, L_{\perp} . We find that the dynamical correlations decay slowly: the zigzag case roughly obeys $\propto 1/L_{\perp}$, while the armchair case shows crossover from $\propto 1/L_{\perp}$ to $\propto 1/L_{\perp}^3$. The results appear to be consistent with the Majorana-mediated spin correlations^{17,19}. Thus, we believe that, when dominated by the itinerant Majorana fermions, the inter-edge dynamical spin correlations become long-range in real space, even in the presence of weak Heisenberg in-

teractions^{37–39}.

Combining these results with the almost constant behaviors of ω_{peak} irrespective of Ω for the other suppressed components in Fig. 5, we conclude that the inter-edge spin resonances in the Kitaev QSL are good probes of two types of fractional excitations, itinerant Majorana fermions and localized fluxes. The resonance in the spin component which does not excite the fluxes on hexagons leads to broad responses with $\omega_{peak} \sim \Omega$, as found in Figs. 5(b) and 5(f). This is a clear indication of the itinerant Majorana excitations. Meanwhile, the responses in the other spin components appear around a small constant ω_{peak} . This is an indication of the gapped flux excitations. We emphasize that weak Heisenberg interactions are essential for the inter-edge spin resonances since all $S_{edge}^{\nu\nu}(\omega)$ vanish for the pure Kitaev model because of the ground-state degeneracy (see Appendix B).

IV. SUMMARY

In summary, we have studied how an AC local magnetic field at an edge of the system induces spin polarizations at the opposite edge in the Kitaev-Heisenberg model with ferromagnetic Kitaev interactions by using the exact diagonalization. We found that in the Kitaev QSL phase the spin polarizations are resonantly induced in a particular spin component, in stark contrast to the magnetically ordered phases where conventional magnetic resonances appear in the transverse spin components. The spin resonance in the Kitaev QSL shows the following peculiar features, stemming from the fractionalization of spin degree of freedom into two types of fractional excitations, itinerant Majorana fermions and localized fluxes: (i) It appears dominantly in the spin component which does not excite flux excitations, (ii) the dominant resonance appears in a broad range of frequency, reflecting the continuum of Majorana excitations, (iii) it is accompanied by subdominant resonances in the other spin components at a small constant frequency corresponding to the flux excitation gap, (iv) both resonances vanish in the exact Kitaev QSL because of the ground-state degeneracy and require weak Heisenberg interactions, and (v) they are induced only dynamically, despite the disappearance of the static spin correlations. While our calculations were done for small size clusters, the inter-edge resonance is expected to be observed in larger systems, since it is mediated by itinerant Majorana excitations that propagate over long distances. These results indicate that the inter-edge dynamical spin resonance is useful for probing the two types of fractional excitations in the Kitaev QSL, which are usually difficult to observe only from static physical quantities.

A straightforward experiment would be implemented by using a scanning tunneling microscope (STM) tip with magnetic atoms or the atomic force microscopy (AFM) to apply an AC magnetic field at the edge and measure the spin polarization at the opposite edge. This could be

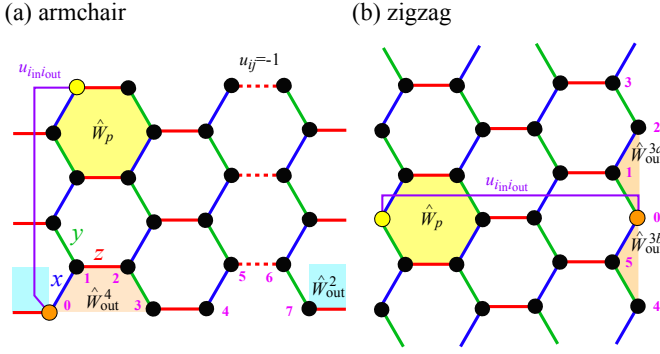


FIG. 9. Schematic pictures of the flux operators for (a) the armchair edges and (b) the zigzag edges. The numbers denote the sites used for the definitions of the fluxes in Eq. (A1) and Eq. (A2). We show examples of the six-spin flux operator \hat{W}_p , four-spin (\hat{W}^4) and two-spin flux operators (\hat{W}^2) and the three-spin flux operators (\hat{W}^{3a} and \hat{W}^{3b}). We also show the inter-edge correlations of the localized Majorana particles ($u_{i_{in}i_{out}}$) by the purple lines. In (a), we represent the z bonds where u_{ij} takes -1 with red dashed lines. See Appendix B for $u_{i_{in}i_{out}}$ and u_{ij} .

performed, for example, for a thin flake of a candidate material α -RuCl₃. Similar experiments would be possible in interface or heterostructure of a Kitaev magnet and a ferromagnetic material, where the AC magnetic field can be applied to the edge spins by the ferromagnetic resonance. Careful analysis of the dynamics in each spin component and its dependence on the edge structure would pave the way for creating and controlling the fractional excitations in the Kitaev QSL through the spin degree of freedom.

ACKNOWLEDGMENTS

We wish to thank Y. Kato, K. Fukui, and T. Okubo for fruitful discussions. This work was also supported by the National Natural Science Foundation of China (Grant No. 12150610462). TM was supported by Building of Consortia for the Development of Human Resources in Science and Technology, MEXT, Japan. This work was supported by Grant-in-Aid for Scientific Research Nos. 19H05825, JP19K03742, and 20H00122 from the Ministry of Education, Culture, Sports, Science and Technology, Japan. It is also supported by JST CREST Grant No. JPMJCR18T2 and JST PRESTO Grant No. JPMJPR19L5.

Appendix A: Degeneracy in the pure Kitaev model with edges

In this Appendix, we show that the ground state of the pure Kitaev model with $\alpha = 3\pi/2$ has the degeneracy

in both cases of the armchair and the zigzag edges. In the pure Kitaev model, one can define the flux operator \hat{W}_p by a product of six spins for each hexagon p , which commutes with the Hamiltonian⁵. We show the examples in Fig. 9; note that \hat{W}_p in (a) [(b)] commutes with $\hat{S}_{i_{in}}^y$ ($\hat{S}_{i_{in}}^z$), since the hexagon lacks the y (z) bond at the i_{in} th site, as discussed in Sec. III B 1 (III B 2). In addition to the six-spin flux operators, at the edges of the system there are additional flux operators defined only by the edge spins. For instance, the flux operators including the output site are given by

$$\hat{W}_{\text{out}}^4 = 2^4 \hat{S}_0^z \hat{S}_1^y \hat{S}_2^z \hat{S}_3^z, \quad \hat{W}_{\text{out}}^2 = 2^2 \hat{S}_0^x \hat{S}_7^y, \quad (\text{A1})$$

for the armchair case, and

$$\hat{W}_{\text{out}}^{3a} = 2^3 \hat{S}_0^x \hat{S}_1^z \hat{S}_2^y, \quad \hat{W}_{\text{out}}^{3b} = 2^3 \hat{S}_0^y \hat{S}_5^z \hat{S}_4^x, \quad (\text{A2})$$

for the zigzag case; see Fig. 9. Since these flux operators \hat{W}^q ($q = 4, 2, 3a$, and $3b$) commute with the Hamiltonian at $\alpha = 3\pi/2$, the ground state $|\Phi_{\text{GS}}\rangle$ is the eigenstate of the flux operators as

$$\hat{W}_{\text{out}}^q |\Phi_{\text{GS}}\rangle = W |\Phi_{\text{GS}}\rangle, \quad (\text{A3})$$

where the eigenvalue W takes +1 or -1. Meanwhile, all the eigenstates of the Hamiltonian can be taken to be real since the Kitaev Hamiltonian does not include the complex elements in the conventional basis set composed of the eigenstates of \hat{S}_i^z . Therefore, if the ground state $|\Phi_{\text{GS}}\rangle$ is unique, we obtain $\langle \Phi_{\text{GS}} | \hat{W}_{\text{out}}^q | \Phi_{\text{GS}} \rangle = 0$ since \hat{W}_{out}^q is the pure imaginary operator including a single \hat{S}_i^y . This contradicts with Eq. (A3), meaning that the assumption of a unique ground state is incorrect. Hence, the ground state of the pure Kitaev model with the armchair and the zigzag edges must be degenerate. For the 24-site clusters shown in Fig. 1, we numerically confirm that the ground state has eightfold (fourfold) degeneracy for the clusters with the armchair (zigzag) edges. We note that the numbers of the degenerate states can be accounted for by the numbers of independent flux-type operators traversing the system from one edge to the other and those consisting of edge spins.

Appendix B: Dynamical spin correlations in the pure Kitaev model

In this Appendix, we describe the method to calculate the dynamical spin correlations for the pure Kitaev model in Figs. 7(a) and 7(c). We adopt the Majorana representation of the Hamiltonian in Eq. (1) at $\alpha = 3\pi/2$, which is given by⁵

$$\hat{\mathcal{H}}_K = \frac{1}{4} \sum_{\langle i,j \rangle_\nu} u_{ij}^\nu i \hat{c}_i \hat{c}_j, \quad (\text{B1})$$

where the spin operator is represented as $\hat{S}_i^\nu = \frac{i}{2} \hat{b}_i^\nu \hat{c}_i$ by introducing four Majorana fermions $\{\hat{c}_i, \hat{b}_i^x, \hat{b}_i^y, \hat{b}_i^z\}$. Here,

$u'_{ij} = \langle \Phi_{\text{GS}} | \hat{u}'_{ij} | \Phi_{\text{GS}} \rangle = \langle \Phi_{\text{GS}} | \hat{i} \hat{b}'_{i_j} \hat{b}'_{j_i} | \Phi_{\text{GS}} \rangle$; \hat{u}'_{ij} commutes with the Hamiltonian and u'_{ij} takes ± 1 .

In this Majorana representation, the inter-edge dynamical spin correlation is given by

$$\begin{aligned} & \langle \Phi_{\text{GS}} | \hat{S}_{i_{\text{in}}}^{\nu}(t) \hat{S}_{i_{\text{out}}}^{\nu} | \Phi_{\text{GS}} \rangle \\ &= -\frac{1}{4} u'_{i_{\text{in}} i_{\text{out}}} \langle \Phi_{\text{GS}} | i \hat{c}_{i_{\text{in}}}(t) \hat{c}_{i_{\text{out}}} | \Phi_{\text{GS}} \rangle, \end{aligned} \quad (\text{B2})$$

where $\nu = y$ and z for the armchair and zigzag case, respectively, and $u'_{i_{\text{in}} i_{\text{out}}}$ is defined for the unpaired $\hat{b}'_{i_{\text{in}}}$ and $\hat{b}'_{i_{\text{out}}}$ on the edges as $u'_{i_{\text{in}} i_{\text{out}}} = \langle \Phi_{\text{GS}} | i \hat{b}'_{i_{\text{in}}} \hat{b}'_{i_{\text{out}}} | \Phi_{\text{GS}} \rangle$. The correlations for the other spin components vanish. By substituting Eq. (B2) to Eq. (8), we obtain the dynamical spin correlation between the edges in the Majorana representation as

$$S_{\text{edge}}^{\text{Maj}}(\omega) = -\frac{u'_{i_{\text{in}} i_{\text{out}}}}{8\pi} \int_{-\infty}^{\infty} \langle \Phi_{\text{GS}} | i \hat{c}_{i_{\text{in}}}(t) \hat{c}_{i_{\text{out}}} | \Phi_{\text{GS}} \rangle e^{i\omega t} dt, \quad (\text{B3})$$

where the time-dependent operator is defined by $\hat{\mathcal{H}}_K$ in which u'_{ij} are chosen to realize the flux-free ground state $|\Phi_0\rangle$: We take all $u'_{ij} = +1$ for the zigzag case, while we flip u'_{ij} to -1 on the z bonds in one column for the armchair case as shown in Fig. 9(a). In both cases, however, the sign of $S_{\text{edge}}^{\text{Maj}}(\omega)$ is indefinite due to the factor of $u'_{i_{\text{in}} i_{\text{out}}}$; we plot the absolute value $|S_{\text{edge}}^{\text{Maj}}(\omega)|$ in Figs. 7 and 8, which corresponds to setting $u'_{i_{\text{in}} i_{\text{out}}} = -1$ in Eq. (B3). Note that Eq. (B3) besides this factor corresponds to the propagator of the Majorana fermions \hat{c}_i .

-
- ¹ E. Majorana, “Teoria simmetrica dell’elettrone e del positrone,” *Il Nuovo Cimento* **14**, 171 (1937).
 - ² F. Wilczek, “Majorana returns,” *Nature Phys* **5**, 614 (2009).
 - ³ A. Kitaev, “Fault-tolerant quantum computation by anyons,” *Annals of Physics* **303**, 2–30 (2003).
 - ⁴ M. Freedman, A. Kitaev, M. Larsen, and Z. Wang, “Topological quantum computation,” *Bulletin of the American Mathematical Society* **40**, 31 (2003).
 - ⁵ A. Kitaev, “Anyons in an exactly solved model and beyond,” *Annals of Physics* **321**, 2 (2006).
 - ⁶ G. Jackeli and G. Khaliullin, “Mott Insulators in the Strong Spin-Orbit Coupling Limit: From Heisenberg to a Quantum Compass and Kitaev Models,” *Phys. Rev. Lett.* **102**, 017205 (2009).
 - ⁷ J. Chaloupka, G. Jackeli, and G. Khaliullin, “Kitaev-Heisenberg Model on a Honeycomb Lattice: Possible Exotic Phases in Iridium Oxides $A_2\text{IrO}_3$,” *Phys. Rev. Lett.* **105**, 027204 (2010).
 - ⁸ R. Yadav, N. A. Bogdanov, Vamshi M. Katukuri, S. Nishimoto, J. Van Den Brink, and L. Hozoi, “Kitaev exchange and field-induced quantum spin-liquid states in honeycomb $\alpha\text{-RuCl}_3$,” *Scientific reports* **6**, 1 (2016).
 - ⁹ Y. Motome and J. Nasu, “Hunting Majorana Fermions in Kitaev Magnets,” *Journal of the Physical Society of Japan* **89**, 012002 (2020).
 - ¹⁰ Y. Kasahara, T. Ohnishi, Y. Mizukami, O. Tanaka, S. Ma, K. Sugii, N. Kurita, H. Tanaka, J. Nasu, Y. Motome, T. Shibauchi, and Y. Matsuda, “Majorana quantization and half-integer thermal quantum Hall effect in a Kitaev spin liquid,” *Nature* **559**, 227 (2018).
 - ¹¹ M. Yamashita, J. Gouchi, Y. Uwatoko, N. Kurita, and H. Tanaka, “Sample dependence of half-integer quantized thermal Hall effect in the Kitaev spin-liquid candidate $\alpha\text{-RuCl}_3$,” *Phys. Rev. B* **102**, 220404(R) (2020).
 - ¹² T. Yokoi, S. Ma, Y. Kasahara, S. Kasahara, T. Shibauchi, N. Kurita, H. Tanaka, J. Nasu, Y. Motome, C. Hickey, S. Trebst, and Y. Matsuda, “Half-integer quantized anomalous thermal Hall effect in the Kitaev material candidate $\alpha\text{-RuCl}_3$,” *Science* **373**, 568 (2021).
 - ¹³ J. A. N. Bruin, R. R. Claus, Y. Matsumoto, N. Kurita, H. Tanaka, and H. Takagi, “Robustness of the thermal Hall effect close to half-quantization in $\alpha\text{-RuCl}_3$,” *Nature Physics* **18**, 401 (2022).
 - ¹⁴ P. Czajka, T. Gao, M. Hirschberger, P. Lampen-Kelley, A. Banerjee, N. Quirk, D. G. Mandrus, S. E. Nagler, and N. P. Ong, “Planar thermal Hall effect of topological bosons in the Kitaev magnet $\alpha\text{-RuCl}_3$,” *Nature Materials*, 1 (2022).
 - ¹⁵ É. Lefrançois, G. Grissonnanche, J. Baglo, P. Lampen-Kelley, J.-Q. Yan, C. Balz, D. Mandrus, S. E. Nagler, S. Kim, Y.-J. Kim, N. Doiron-Leyraud, and L. Taillefer, “Evidence of a Phonon Hall Effect in the Kitaev Spin Liquid Candidate $\alpha\text{-RuCl}_3$,” *Phys. Rev. X* **12**, 021025 (2022).
 - ¹⁶ A. J. Willans, J. T. Chalker, and R. Moessner, “Site dilution in the Kitaev honeycomb model,” *Phys. Rev. B* **84**, 115146 (2011).
 - ¹⁷ A. Koga, Y. Murakami, and J. Nasu, “Majorana correlations in the Kitaev model with ordered-flux structures,” *Phys. Rev. B* **103**, 214421 (2021).
 - ¹⁸ G. Baskaran, S. Mandal, and R. Shankar, “Exact Results for Spin Dynamics and Fractionalization in the Kitaev Model,” *Phys. Rev. Lett.* **98**, 247201 (2007).
 - ¹⁹ T. Minakawa, Y. Murakami, A. Koga, and J. Nasu, “Majorana-Mediated Spin Transport in Kitaev Quantum Spin Liquids,” *Phys. Rev. Lett.* **125**, 047204 (2020).
 - ²⁰ A. J. Willans, J. T. Chalker, and R. Moessner, “Disorder in a Quantum Spin Liquid: Flux Binding and Local Moment Formation,” *Phys. Rev. Lett.* **104**, 237203 (2010).
 - ²¹ D. Takikawa, M. G. Yamada, and S. Fujimoto, “Dissipationless spin current generation in a Kitaev chiral spin liquid,” *Phys. Rev. B* **105**, 115137 (2022).
 - ²² M. O. Takahashi, M. G. Yamada, M. Udagawa, T. Mizushima, and S. Fujimoto, “Non-local spin corre-

- lation as a signature of Ising anyons trapped in vacancies of the Kitaev spin liquid,” [arXiv preprint arXiv:2211.13884 \(2022\)](#).
- ²³ J. Feldmeier, W. Natori, M. Knap, and J. Knolle, “Local probes for charge-neutral edge states in two-dimensional quantum magnets,” *Phys. Rev. B* **102**, 134423 (2020).
- ²⁴ E. J. König, M. T. Randeria, and B. Jäck, “Tunneling Spectroscopy of Quantum Spin Liquids,” *Phys. Rev. Lett.* **125**, 267206 (2020).
- ²⁵ R. G. Pereira and R. Egger, “Electrical Access to Ising Anyons in Kitaev Spin Liquids,” *Phys. Rev. Lett.* **125**, 227202 (2020).
- ²⁶ M. Udagawa, S. Takayoshi, and T. Oka, “Scanning Tunneling Microscopy as a Single Majorana Detector of Kitaev’s Chiral Spin Liquid,” *Phys. Rev. Lett.* **126**, 127201 (2021).
- ²⁷ K. Klocke, D. Aasen, R. S. K. Mong, E. A. Demler, and J. Alicea, “Time-Domain Anyon Interferometry in Kitaev Honeycomb Spin Liquids and Beyond,” *Phys. Rev. Lett.* **126**, 177204 (2021).
- ²⁸ Z. Wei, V. F. Mitrović, and D. E. Feldman, “Thermal Interferometry of Anyons in Spin Liquids,” *Phys. Rev. Lett.* **127**, 167204 (2021).
- ²⁹ S.-H. Jang, Y. Kato, and Y. Motome, “Vortex creation and control in the Kitaev spin liquid by local bond modulations,” *Phys. Rev. B* **104**, 085142 (2021).
- ³⁰ Y. Liu, K. Slagle, Kenneth S. Burch, and J. Alicea, “Dynamical anyon generation in Kitaev honeycomb non-Abelian spin liquids,” [arXiv:2111.09325 \(2021\)](#).
- ³¹ A. P. Joy and A. Rosch, “Dynamics of Visions and Thermal Hall Effect in Perturbed Kitaev Models,” *Phys. Rev. X* **12**, 041004 (2022).
- ³² C. Chen and I. S. Villadiego, “Nature of visons in the perturbed ferromagnetic and antiferromagnetic Kitaev honeycomb models,” *Phys. Rev. B* **107**, 045114 (2023).
- ³³ J. Chaloupka, G. Jackeli, and G. Khaliullin, “Zigzag Magnetic Order in the Iridium Oxide Na_2IrO_3 ,” *Phys. Rev. Lett.* **110**, 097204 (2013).
- ³⁴ M. Kawamura, K. Yoshimi, T. Misawa, Y. Yamaji, S. Todo, and N. Kawashima, “Quantum lattice model solver $\text{H}\Phi$,” *Computer Physics Communications* **217**, 180 (2017).
- ³⁵ The data for $S^z(\omega_{\text{peak}})$ at $\Omega = 2\pi/10 \simeq 0.63$ and $S^z(\omega_{\text{peak}})$ at $\Omega = 2\pi/5 \simeq 1.26$ in the armchair case deviate from the constant behavior, and rather close to Ω . In these cases, we also observe peaks around the constant values, but the peak heights are slightly smaller than those around Ω .
- ³⁶ J. Knolle, D. L. Kovrizhin, J. T. Chalker, and R. Moessner, “Dynamics of a Two-Dimensional Quantum Spin Liquid: Signatures of Emergent Majorana Fermions and Fluxes,” *Phys. Rev. Lett.* **112**, 207203 (2014).
- ³⁷ K. S. Tikhonov, M. V. Feigel’man, and A. Yu. Kitaev, “Power-law spin correlations in a perturbed spin model on a honeycomb lattice,” *Phys. Rev. Lett.* **106**, 067203 (2011).
- ³⁸ S. Mandal, Subhro Bhattacharjee, K. Sengupta, R. Shankar, and G. Baskaran, “Confinement-deconfinement transition and spin correlations in a generalized Kitaev model,” *Phys. Rev. B* **84**, 155121 (2011).
- ³⁹ X.-Y. Song, Y.-Z. You, and L. Balents, “Low-Energy Spin Dynamics of the Honeycomb Spin Liquid Beyond the Kitaev Limit,” *Phys. Rev. Lett.* **117**, 037209 (2016).